# RSC Advances

This is an *Accepted Manuscript*, which has been through the Royal Society of Chemistry peer review process and has been accepted for publication.

*Accepted Manuscripts* are published online shortly after acceptance, before technical editing, formatting and proof reading. Using this free service, authors can make their results available to the community, in citable form, before we publish the edited article. This *Accepted Manuscript* will be replaced by the edited, formatted and paginated article as soon as this is available.

You can find more information about *Accepted Manuscripts* in the Information for Authors.

Please note that technical editing may introduce minor changes to the text and/or graphics, which may alter content. The journal's standard Terms & Conditions and the Ethical guidelines still apply. In no event shall the Royal Society of Chemistry be held responsible for any errors or omissions in this *Accepted Manuscript* or any consequences arising from the use of any information it contains.

ROYAL SOCIETY OF CHEMISTRY

www.rsc.org/advances

# Effects of intrinsic defects and extrinsic doping on the electronic and photocatalytic properties of $Ta_3N_5$

Tao Jing,[a,b] Ying Dai,[*a] Xiangchao Ma,[a] Wei Wei,[a] and Baibiao Huang[a]
a School of Physics, State Key Laboratory of Crystal Materials, Shandong University, Jinan 250100, People's Republic of China
b College of Physics and Electronic Engineering, Kaili University, Kaili Guizhou 556011, People's Republic of China
*E-mail: daiy60@sina.com

**Abstract** $Ta_3N_5$ can be a good candidate of oxygen evolution photocatalyst or a photoanode for Z-scheme device due to its n-type feature. In the present work, the formation energies and electronic structures of defects contained $Ta_3N_5$ are studied by first principles density functional method in details. Our results show that the substitution of O for three-coordinated N in $Ta_3N_5$ possesses low formation energy and introduces a shallow donor under both N-rich and N-poor conditions, making the most contribution to the n-type conductivity. By the optical transition levels, we show that the four-coordinated N vacancy in $Ta_3N_5$ is responsible for the observed 720nm sub-band gap optical absorption. In addition, for alkali metal doped $Ta_3N_5$, our results reveal that the interstitial doping can lead to enhanced conductivity and reduced band gap, and the doping of Na and K in $Ta_3N_5$ are expected to produce higher photocatalytic activity compared to Rb and Cs. These results are useful to understand the recent experimental observations and provide a guidance to engineer $Ta_3N_5$ for improving photocatalytic efficiencies.

## 1 Introduction

The direct splitting of water into oxygen and hydrogen by semiconductor photocatalysts



RSC Advances Accepted Manuscript

has been proposed as a clean and renewable approach to resolve the global energy and environment crisis.[1-3] However, most of the photocatalytic materials possessing the ability to split water allow only UV optical absorption, which greatly restricts their energy conversion efficiency. Aiming at improving the utilization of solar energy, thus, numerous studies have focused on semiconductor materials possessing narrow band gap.[4-7] It is unanimously accepted that an ideal semiconductor material for the photoelectrode should have a suitable band gap of about 2.0 eV to meet both the dynamic reaction barrier and a wide range of optical absorption. Meanwhile, the conduction band and valence band edges of the semiconductor should straddle the water redox potentials in order to split water without external bias. Therefore, transition metal (oxy)nitrides such as $LaTaO_2N$[8-10] and $Ta_3N_5$[11-14], have attracted massive research interest during the past decades because of the suitable band gap and band edge positions. Despite that great effort has been taken to improve photocatalytic performance, several challenges still remain including stabilizing the surface against photooxidation and improving the quantum yield.

Due to the n-type feature, $Ta_3N_5$ can be applied as an oxygen evolution photocatalyst or a photoanode for Z-scheme device.[15] Generally, for metal oxides and nitrides such as $TiO_2$ and GaN, the most common origin of the n-type conductivity is attributed to anion vacancies.[16] But there are a number of exceptions. For example, previous theoretical calculation indicated that $O_N$ anti-site, as a dominant intrinsic defect in TaON, is responsible for its n-type conductivity.[17] On the other hand, some experimental studies reported that O defects as unintentional impurities are included in $Ta_3N_5$ inevitably during the synthesis even under the anaerobic condition.[18,19] Thus, the oxygen defects may potentially contribute to the n-type



RSC Advances Accepted Manuscript

conductivity in $Ta_3N_5$. Previous theoretical calculation has also shown that the formation energy of O substituting for N is smaller than N vacancy.[20] However, few theoretical studies focus on the n-type conductive behavior of $Ta_3N_5$, in particular, the effect of the oxygen defects on this property. It is known that extrinsic doping is an effective approach to improve the n-type conductivity of semiconductor materials, which can enlarge the band bending and facilitate the migration of holes from bulk to surface. Therefore, the quantum yield of $Ta_3N_5$ can be improved by enhanced n-type conductivity. Indeed, It is previously observed that alkali metal (Na, K, Rb, Cs) doped $Ta_3N_5$ has enhanced activity for photocatalytic splitting water.[21-23] The main doping effects are a lower band gap and a drastic enhancement in the electrode conduction. Among these materials, Na doped $Ta_3N_5$ has the highest improvement of photocatalytic activity.[23] Nevertheless, the origin of reduced band gap and enhanced conductivity is still need to further investigate.

In this work, aiming at solving the questions shown above, the formation energies and electronic structures of various intrinsic and extrinsic defect contained $Ta_3N_5$ are investigated by first principles calculation. Our results show that the substitution of O for three-coordinated N is the most stable among all of the defects in $Ta_3N_5$ considered here, and is mainly responsible for the n-type conductivity. Despite the different characteristics of electronic structure, both two types of N vacancies have shallow thermodynamic transition level of (0/+1). In addition, the interstitial doping of alkali metals in $Ta_3N_5$ can produce an enhanced n-type conductivity. Na and K are better donors over Sr and Cs, leading to higher enhancement of electronic conductivity and photocatalytic activity. The reduced band gap of alkali metal doped $Ta_3N_5$ can be attributed to large lattice distortion induced by interstitial



RSC Advances Accepted Manuscript

doping.

## 2 Computational details

The spin-polarized density function theory (DFT) calculations were performed by the Vienna ab initio simulation package (VASP).[24] The projector augmented wave (PAW) method was applied for the interactions between the valence electrons and the ionic cores. Generalized gradient approximation (GGA) in the formulation of Perdew-Burke-Ernzerhof (PBE) was employed for exchange-correlation functional.[25] The electron wave function was expanded in a basis set of plane waves with a kinetic energy cut off of 500eV. We simulated the doping effects using a 3×1×1 repetition of the $Ta_3N_5$ unit bulk cell with 96-atom, and a 3×3×3 Monkhorst-Pack k-point set were used to obtain the accurate geometry and electronic structure.[26] The lattice parameters and the atomic positions were fully relaxed until that all forces are smaller than 0.01 eV/Å, and the convergence threshold for self-consistence field iteration was set at $10^{-6}$eV.

The formation energy of a defect α in charge state q is given by[27,28]

$$H_f(\alpha, q) = E(\alpha, q) - E(bulk, 0) + \Sigma ni\mu i + qE_f + \Delta V$$

Where $E(\alpha,q)$ is the total energy of defects contained $Ta_3N_5$ supercell in charge state $q$, $E(bulk,0)$ is the total energy of a perfect crystal in the same supercell. $\mu i$ ($i$=Ta, N or O) refers to the atomic chemical potential of the type i atoms, and $ni$ is the number of atoms of type $i$ added to ($ni$<0) and/or removed from ($ni$>0) the perfect crystal. $E_f$ is the Fermi level referenced to the valence band maximum (VBM). $\Delta V$ is the VBM correction term, which can be obtained by aligning the average electrostatic potentials between the defect contained supercell and the defect-free supercell. The electrostatic interactions between the defects



RSC Advances Accepted Manuscript

resulting from the periodic supercell cannot be neglected.[27] Previous theoretical studies have shown that the first-order Makov-Payne correction can be used to removed such spurious electrostatic interaction.[29,30] However, its reliability and generality remain controversial. Here, we correct the defect formation energies by using the extrapolation method, more details are given in Fig S1(in supporting information). The thermodynamic transition level of $\varepsilon_D(q/q^0)$ for a given defect, corresponding to the positions of Fermi level at which a given defect changes from charge state $q$ to $q^0$, can then be written as

$$\varepsilon_\alpha(q/q^0) = {H_f(\alpha,q) - H_f(\alpha,q^0)} \big/ {(q^0 - q)}$$

Owing to the all known band gap underestimation of DFT, we carried out a DFT plus on-site repulsion U (DFT+ U) scheme with U=0.06eV on N 2p states, 3.96 eV on O 2p and 6.47 eV on Ta 5d, since previous theoretical studies demonstrated that it given a reasonable and reliable description for the electron structures of $Ta_3N_5$.[20] Here, our calculated band gap is 2.07eV, which is in good consistence with the experimental value of 2.1eV. For alkali metal elements, no +U correction was required.

## 3 Result and discussion

### 3.1 Chemical potentials

In generally, the defect formation energies are affected by element chemical potentials during the process of growth. Thus, to avoid the precipitation of element phases, a thermodynamic limit is proposed for the chemical potentials under equilibrium growth conditions

$$\mu_N \leq 0, \mu_{Ta} \leq 0$$



RSC Advances Accepted Manuscript

To keep $Ta_3N_5$ thermodynamically stable, it is required that $\mu_{Ta3N5} = 3\mu_{Ta} + 5\mu_N$, the calculated $\mu_{Ta3N5}$ value is -9.96eV, which is in consistence with other theoretical values of 9.74 eV (GGA+U)[20] and 9.45 eV (hybrid functional method)[18]. In order to avoid the formation of secondary phases during the growth of $Ta_3N_5$, the following conditions should be satisfied

$$\mu_{Ta} + \mu_N < \mu_{TaN} = -1.55eV,$$

$$5\mu_{Ta} + 6\mu_N < \mu_{Ta_5N_6} = -12.57eV,$$

As shown in Fig 1, the calculated accessible ranges of chemical potentials for different elements are plotted in a two-dimensional ($\mu_{Ta}$ and $\mu_N$) plane. The blue line refers to the allowed range of chemical potentials of Ta and N for forming $Ta_3N_5$. Two specific chemical potential points of A and B, referring to N-rich and N-poor conditions, respectively, are adopted to calculate defect formation energies. For condition A, chemical potentials of $\mu_{Ta}$ and $\mu_N$ are -3.32eV and 0, respectively; while they are -0.44 and -1.73 eV for condition B. Considering that O atoms are included in $Ta_3N_5$ unavoidably in the process of growth, the secondary phases such as TaON and $Ta_2O_5$ should also be avoided,

$$\mu_{Ta} + \mu_O + \mu_N < \mu_{TaON} = -6.1eV,$$

$$2\mu_{Ta} + 5\mu_O < \mu_{Ta_2O_5} = -18.18eV,$$

In $Ta_3N_5$, there are two types of symmetrically different N, which are denoted as $N_3$ (the N three-coordinated with Ta) and $N_4$ (the N four-coordinated with Ta). In this study, the following defects are taken into account: Ta vacancy ($V_{Ta}$), N vacancy ($V_{N3}$ and $V_{N4}$), N interstitial ($N_i$), Ta interstitial ($Ta_i$). The cation/anion anti-site defects, such as Ta on the N site and N on the Ta site, are not considered in this study due to their large formation energies.



RSC Advances Accepted Manuscript

Because of the involvement of O element, the defects of O interstitial ($O_i$) and substitution of O for N ($O_{N3}$ and $O_{N4}$) are also contained in our calculations. Additionally, for the alkali metal doping, only cationic substitution and interstitial doping are included in our defect investigation.

## 3.2 Formation energies and transition levels for intrinsic defects

The formation energies of point defects in $Ta_3N_5$ as a function of the Fermi level in the two chosen chemical potential environments A and B are given in Figure 2. Under N rich condition, as shown in Fig 2a, we can see that $O_{N3}$ is the most stable defect in almost the whole range of band gap. $N_i$ is easier to form when the Fermi level is close to the conduction band minimum, and the Fermi level will be pinned at 0.11eV below the CBM by the charge neutrality between positively and negatively charged defects in the absence of other extrinsic dopants in $Ta_3N_5$.[31] In addition, both $O_{3N}$ and $O_{4N}$ being shallow donors, are stable only in +1 charge state, and $O_{N4}$ possesses higher formation energy compared to $O_{N3}$ with a difference value of 0.27eV, which is slightly smaller than previous reported theoretical value of 0.56eV.[18] Thus, the $O_{N3}$ is responsible for the n-type conductivity of $Ta_3N_5$. The calculated DOS indicates that the defect states induced by O are resonant with the conduction band, as shown in Fig 3a and 3b, this is understandable because of the lower energy of O 2p compared to N 2p orbital. Therefore, based on above analysis, the involvement of $O_N$ defects in $Ta_3N_5$ is extremely advantageous for the improvement of n-type conductivity and can thus lead to the enhanced photocatalytic activity for $Ta_3N_5$.

For the N vacancy defects, as shown in Fig 2a, it is noted that both $V_{N3}$ and $V_{N4}$ can be



RSC Advances Accepted Manuscript

stable in +1, +2 and +3 charge states depending on the position of Fermi level, $V_{N4}$ has lower formation energy compared to $V_{N3}$ when the Fermi level is high in the band gap, otherwise $V_{N3}$ is more stable. In addition, the ionization levels of (0/+1) for both $V_{N3}$ and $V_{N4}$ are above the CBM, implying shallow donor property. Whereas the (+1/+2) and (+2/+3) levels of $V_{N3}$ are located in the band gap with the values of 0.91 and 1.11eV below the CBM, respectively, while those of 1.36 and 1.48eV for $V_{N4}$. To examine the origin of the shallow (0/+1) ionization levels, the calculated DOS of neutral N vacancy defects is given in Fig 3c and 3d. $V_{N4}$ defect in $Ta_3N_5$ creates two localized deep states within the band gap and a delocalized state resonating with the conduction band, thereby this delocalized state will be responsible for the shallow character of (0/+1) ionization level of $V_{N4}$ defect.[28] To further investigate the defect state distribution, we perform the calculation of decomposed charge density, as plotted in Fig 4. Indeed we note that upon the removal of $N_4$ atom in $Ta_3N_5$, correspondingly three electrons are released, two electrons are trapped by Ta dangling bonds neighboring the N vacancy, while the other one distributes in a large volume, which is characterized by delocalized states. This picture is consistent with the DOS analysis above. On the contrary, the DOS shown in Fig 3d reveals that $V_{N3}$ does not exhibit conventional shallow donor behavior, and three deep localized defect states appear in the band gap. The decomposed charge density shown in Fig 4b also provides evidence that the three electrons are mainly localized on the Ta dangling bonds around the $N_3$ vacancy. To investigate how the shallow donor level is produced, the relaxation energy has been calculated since the thermodynamics transition level is not only in relation to the position of electronic states but also to the relaxation energy after electron transition.[32] Here, the relaxation energy is defined as the



RSC Advances Accepted Manuscript

energy difference of $V_N$ defect at +1 charge state between $V_N^{+1}$ and $V_N^0$ atomic geometries. As expected, the calculated value for $V_{3N}^{+1}$ is 0.37eV, which is significantly larger than the value of 0.08eV for $V_{4N}^{+1}$. However, this value is still not enough to explain so large difference between the positions of defects states and ionization levels of (0/+1) for $V_{N3}$ vacancy, we attribute it to large Coulomb repulsion interaction between these localized electrons. By further examination of the geometry structure of $V_{N3}$ defect, it is found that the Ta atoms around the N vacancy move out by about 1.7% after one electron was ionized, it is remarkably larger compared to $V_{N4}$, which has only 0.22% relaxation, indicating that a larger geometric relaxation can be realized for $V_{N3}$ after one electron is ionized compared to that of $V_{N4.}$ As mentioned above, the $V_{N3}$ and $V_{N4}$ defects can contribute to n-type conductivity to some extent due to the shallow nature of (0/+1) level. However, the deep levels of (+1/+2) and (+2/+3) make these defects acting as recombination center in $Ta_3N_5$, which is harmful for photocatalytic activity.[33]

As shown in Fig 2a, the interstitial N in $Ta_3N_5$ is stable only in +1 and -1 charge states with the (-1/+1) transition level at 0.58eV above the VBM, indicating that it is a negative U defect.[34] Therefore, it cannot contribute to the n-type conductivity because it behaves like an acceptor under typical n-type conditions while as a donor under p-type conditions. From the DOS shown in Fig 5a, we note that $N_i$ introduces two impurity states in the band gap with an occupied one near the VBM and an unoccupied state in middle of band gap. In order to further explore its electronic structure information, the local geometric structure of $N_i$ is given in Fig 6a. We can see that the most stable $N_i$ structure is the split configuration,[35] which refers to the interstitial N atom sharing the same site with a three-coordinated N atom. Based



RSC Advances Accepted Manuscript

on molecular orbital theory, we propose a model for the local bonding shown in Fig 7a. Because of the similar energies of the 2p orbitals, the coupling between the two N atoms is so strong that unoccupied $\sigma_u$ anti-bonding orbital is located above the CBM, and a singly occupied $\pi_g$ anti-bonding in the band gap. Therefore, these defect states can accept an additional electron from the valance band or donate an electron into the conduction band, explaining both acceptor and donor properties of $N_i$ defect. The interstitial O is stable in neutral charge state across almost whole band gap as shown in Fig 2a, the donor level (+1/0) is extremely deep, which is at about 2 eV below the CBM. In order to reveal the origin of completely different characteristics between the two interstitial defects, a closer look at the electronic structure is helpful. Figure 5b shows the absence of defect state in the band gap and the Fermi level just located at VBM. Because of the similar geometry structure as $N_i$, shown in Fig 6b, the local bonding structure based on molecular orbital theory are given in Fig 7b. The lower energy of O 2p compared to N 2p, means that the $\pi_g$ antibonding orbital of O-N bond is not as strong as N-N bond, resulting in these states within the valance band. A similar split configuration has been reported for interstitial N doped $TiO_2$ by previous theoretical investigation, however, the transition levels of (-1/+1) are located at 1.54 eV and 1.98 eV above VBM for anatase and rutile, respectively.[35] We attribute such difference to that the VBM of $Ta_3N_5$ is higher in energy compared to $TiO_2$.

The interstitial Ta is stable in +1, +2, +3, +4 and +5 charge states depending on the position of Fermi level, and the transition levels of (+1/+2), (+2/+3), (+3/+4) and (+4/+5) are at 0.05, 0.55, 0.67 and 1.11eV below the CBM, respectively. $Ta_i$ can donate one electron to the conduction band spontaneously. Nevertheless, the large formation energy implies low



RSC Advances Accepted Manuscript

concentration of this defect in $Ta_3N_5$, thus making slight contribution to its n-type conductivity. Similarly, owning to the extremely large formation energy, Ta vacancy is unlikely to form in $Ta_3N_5$ during growth and we will not discuss it in details.

Under N poor condition, as shown in Fig 2b, the positions of thermodynamic transition levels are essentially not changed. However, the formation energies of donor defects are significantly lower compared to that in N rich condition, while the formation energies of the acceptors are increased. $O_{N3}$ has the lowest formation energy even in whole range of band gap and no acceptor can compensate for it, implying that a stronger n-type conductivity can been obtained during synthesis under this condition. In addition, the formation energies of donor defects such as $V_N$ and $Ta_i$, whose donor levels are deep in the band gap, decrease with downshift of the N chemical potential, which can increase the sub-band gap light absorption of $Ta_3N_5$. Indeed, the increase of sub-band gap absorption and charge mobility has been observed from the synthesized $Ta_3N_5$ samples with rising nitridation temperature from 850°C to 1000°C.[36]

The previous experimental studies have revealed a 720nm optical absorption by UV-Vis optical absorption spectra measurement, the origin of which was assigned to the reduced $Ta^{5+}$ ions.[18] The investigation taken by A. Dabirian has implied that nitrogen vacancy is the most probably candidate for the 720 nm light absorption.[37] To provide an assignment for these optical absorption spectra, the optical transition level is calculated since it has been shown to give very good description for experimental optical absorption.[35,38,39] Herein we only consider the N-rich condition since consistent conclusion can be obtained under the two growth conditions. As discussed before, the Fermi level locates at 0.11eV below the CBM,



RSC Advances Accepted Manuscript

thus, the stable charge states of both $V_{N4}$ and $V_{N3}$ are +1, while for $N_i$ and $Ta_i$ they are -1 and +2, respectively. $O_N$ and $O_i$ are unlikely to cause this optical absorption and thus not included in our calculations. Based on the Frank-Condon principle, we can calculate the possible optical transitions associated with these defects. To explain the transitions process qualitatively, for $V_{N4}$, the configuration coordinate diagram is shown in Fig 8a.[39] Here $V_{N4}^{+1}$ is considered as the ground state while $V_{N4}^{+2}$ as the excited state. As discussed before, the thermodynamic transition levels is 1.36eV below the CBM. Considering an electron transition from defect state to the conduction band after absorption of a photon, the charge state of $V_{N4}$ will be changed from +1 to +2, while the atomic geometry is still kept in that of +1 charge state because the light absorption process is far more quickly than the corresponding lattice relaxation. The optical transition level (+1/+2) is defined as the crossing point of the formation energies between $V_{N4}^{+1}$ charge state in $V_{N4}^{+1}$ atomic geometry and $V_{N4}^{+2}$ charge state in $V_{N4}^{+1}$ atomic geometry, as shown in Fig 8b. Our calculated optical transition energy is 1.71eV, which is in excellent agreement with the experimental report of 1.72eV.[18,37] The defect relaxation energy, defined as the difference between optical transition energy and thermodynamic transition energy, is thus about 0.35eV. Moreover, the optical transition energies for other defects are also calculated. For $V_{N3}$, our calculated value is 1.38eV. It means that the two types of N vacancy have large difference in sub-band gap optical absorption. For $N_i$, by considering optical transition: $N_i^{-1} \rightarrow N_i^{0}$, the calculated value is 2.07eV, while the optical transition of $Ta_i^{+2} \rightarrow Ta_i^{+3}$ for $Ta_i$ is 0.89eV. Therefore, our results consistently show that the optical transition $V_{N4}^{+1} \rightarrow V_{N4}^{+2}$ is responsible for the experimental observed 720nm optical absorption.



RSC Advances Accepted Manuscript

### 3.3 The doping effects on photocatalytic properties of $Ta_3N_5$

Finally, to explain the origin of enhanced conductivity and reduced band gap of $Ta_3N_5$ through doping of alkali metals, their corresponding formation energies and electronic structure are also investigated. Since the growth temperatures of $Ta_3N_5$ are commonly high and the alkali metal nitrides are expected to dissociate at such high temperatures, the relevant secondary phases can be excluded. Thus, only the metal phases are adopted for their chemical potential calculation. To examine the origin of the enhanced conductivity, firstly, the formation energies of alkali metals (Na, K, Rb, Cs) doped $Ta_3N_5$ as a function of Fermi level are given in Fig S2. Because the formation energies of cationic substitution doping are found to be remarkable high, only interstitial doping are shown herein. Indeed, we note that the thermodynamic transition levels for all of the alkali metal interstitial defects are very shallow and these defects are stable only in +1 charge state, indicating their excellent donor properties. Thus, these results provide a basis for elucidating the enhanced conductivity of alkali metal doped $Ta_3N_5$ revealed by experiment studies.[21-23] Moreover, the defect formation energies satisfy this order: Na > K > Rb > Cs. It implies that Na and K have larger solubility in $Ta_3N_5$, leading to more excellent conductivity compared to others, which is in good agreement with the experimental observation.[23] Due to the larger ions radius of Rb and Cs compared to Na and K, the incorporation of these elements can lead to larger lattice distortion in $Ta_3N_5$, thereby, the higher formation energies are required.

To further investigate the cause of the reduced band gap, the DOS of alkali metal doped $Ta_3N_5$ are shown in Fig S3. Due to higher energies of the s orbitals of alkali metal compared



RSC Advances Accepted Manuscript

to Ta 5d orbital, the alkali metal states make almost no contribution to band edges, one excess electron is therefore easily donated into the conduction band of $Ta_3N_5$, narrating the shallow donor nature of these defects. The calculated band gap of Na, K, Rb and Cs doped $Ta_3N_5$ are 2.02, 2.01, 1.96 and 1.85eV, respectively. Compared with pure $Ta_3N_5$, the incorporation of Na and K ions results in slight reduction of band gap, while Cs doping significantly reduce the band gap. which is close to the experimentally reported range of 1.7-1.8eV.[23] Since the ionic radius of Cs atom is the largest among these alkali metal elements, we point out that the lattice distortion induced by doping is expected to affect the electronic structure and reduce the band gap of $Ta_3N_5$. On the basis of the above analysis, higher concentrations of Na and K doping are considered by incorporating one or two atoms in 2×1×1 (64 atom) $Ta_3N_5$ supercell, corresponding to 1.6 and 3.1% atomic concentrations, respectively. Such high doping concentrations are reasonable since Na and K doped $Ta_3N_5$ have lower defect formation energies. The calculated band gap are 1.94 and 1.97eV for 1.6% atomic concentration of Na and K, respectively, 1.60 and 1.72eV for 3.1% atomic concentration, which are in excellent agreement with experimental reports.[22,23]

In general, the prepared $Ta_3N_5$ shows n-type conductivity and is often used for splitting water to produce oxygen. The improvement of conductivity is an effective strategy to enhance the activity of photocatalytic materials. For example, previous experimental studies suggested that the substitution of Mo or W at V sites in $BiVO_4$ could lead to remarkable improvement of conductivity and promote internal charge separation.[40,41] As shown in this paper, the interstitial doping of alkali metals in $Ta_3N_5$ could effectively increase the carrier concentration and reduce its band gap to some extent. Moreover, the incorporation of atoms



RSC Advances Accepted Manuscript

with smaller ionic radius can lead to higher doping concentration and thus larger enhancement of conductivity. Recently, Ba doped $Ta_3N_5$ has been synthesized, yielding a maximum solar energy conversion efficiency of 1.5%, the enhanced activity was assigned to the synergistic effects of enhanced interlayer conductivity.[42] Based on our previous results, thus, doping of alkaline-earth metal, such as Mg, Ca and Sr in $Ta_3N_5$, may also lead to improvement of electronic conductivity to achieve higher photocatalytic efficiency since they possess smaller ionic radius than Ba. Although Mo and W have one more valence electron than Ta, the energies of their d orbitals are lower than that of Ta.[43] Therefore, the substitution of Mo or W for Ta in $Ta_3N_5$ is not good selections for improving the photocatalytic performance.[44] Our results can serve as a guidance to engineer $Ta_3N_5$ for improving photocatalytic efficiencies.

## 4 Conclusion

In summary, we investigated the formation energies and electronic structures of intrinsic and extrinsic defects contained in $Ta_3N_5$ by first principles calculations, our results demonstrated that:

(1)$O_{N3}$ in $Ta_3N_5$ is the dopant with the lowest formation energy and excellent donor properties among the studied defects, making the most contribution to its n-type conductivity. In addition, higher carrier concentration can be obtained under N-poor condition; Despite the different features of defect states, both $V_{N3}$ and $V_{N4}$ have a shallow (0/+1) level; N and O interstitial defects in $Ta_3N_5$ can form a split configuration, $N_i$ possesses both donor and acceptor properties, while $O_i$ only act as a deep donor.

(2)The results of optical transition levels show that the sub-band gap light absorption



RSC Advances Accepted Manuscript

around 720 nm could be assigned to the optical transition $V_{N4}^{+1} \rightarrow V_{N4}^{+2}$, while $V_{N3}$, possessing lower absorption energy and higher defect formation energy, is unlikely to contribute to this range of light absorption.

(3)Alkali metals interstitial doping in $Ta_3N_5$ can lead to enhanced conductivity due to their shallow donor properties, the reduced band gap can be attributed to the lattice distortion induced by interstitial doping. In addition, due to the lower formation energy of Na compared to others, it can lead to larger improvement in conductivity and photocatalytic activity. The present work may provide an effective strategy to improve the photocatalytic activity of $Ta_3N_5$.

## Acknowledgement

This work is supported by the National Basic Research Program of China (973 program, 2 013CB632401), National Science foundation of China under Grant11374190, 21333006, and 11404187 and 111 Project B13029. We also thank the National Supercomputer Center in Jinan for providing high performance computation.

## References

1 A. Kudo and Y. Miseki, *Chem. Soc. Rev.*, 2009, **38**, 253–278.

2 X. Chen, S. Shen, L. Guo and S. S. Mao, *Chem. Rev.*, 2010, **110**, 6503–6570.

3 H. Tong, S. Ouyang, Y. Bi, N. Umezawa, M. Oshikiri and J. Ye, *Adv. Mater.*, 2012, **24**, 229–251.

4 Y. Bi, S. Ouyang, N. Umezawa, J. Cao and J. Ye, *J. Am. Chem. Soc.*, 2011, **133**, 6490–6492.

5 F. E. Osterloh, *Chem. Soc. Rev.*, 2013, **42**, 2294–2320.



RSC Advances Accepted Manuscript

6 P. Wang, B. B. Huang, X. Y. Qin, X. Y. Zhang, Y. Dai, J. Y. Wei and M.-H. Whangbo, *Angew. Chem., Int. Ed.*, 2008, **47**, 7931–7933.

7 X. Ma, Y. Dai, B. B. Huang, *ACS Appl. Mater. Interfaces*, 2014, **6**, 22815–22822.

8 A. Kasahara, K. Nukumizu, G. Hitoki, T. Takata, J. N. Kondo, M. Hara, H. Kobayashi and K. Domen, *J. Phys. Chem. A*, 2002, **106**, 6750–6753.

9 C. L. M. Leroy, A. E. Maegli, K. Sivula, T. Hisatomi, N. Xanthopoulos, E. H. Otal, S. Yoon, A. Weidenkaff, R. Sanjinesd and M. Gratzel, *Chem. Commun.*, 2012, **48**, 820–822.

10 W. Luo, Z. Li, X. Jiang, T. Yu, L. Liu, X. Chen, J. Ye and Z. Zou, *Phys. Chem. Chem. Phys.*, 2008, **10**, 6717–6723.

11 W. J. Chun, A. Ishikawa, H. Fujisawa, T. Takata, J. N. Kondo, M. Hara, M. Kawai, Y. Matsumoto and K. Domen, *J. Phys. Chem. B*, 2003, **107**, 1798–1803.

12 P. Zhang, J. Zhang and J. Gong, *Chem. Soc. Rev.*, 2014, **43**, 4395–4422.

13 C. Zhen, L. Wang, G. Liu, G. Q. Lu and H.-M. Cheng, *Chem. Commun.*, 2013, **49**, 3019–3021.

14 J. Wang, J. Feng, L. Zhang, Z. Li and Z. Zou, *Phys. Chem. Chem. Phys.*, 2014, **16**, 15375–15380.

15 S. S. K. Ma, K. Maeda, T. Hisatomi, M. Tabata, A. Kudo and K. Domen, *Chem.–Eur. J.*, 2013, **19**, 7480–7486.

16 B. J. Morgan and G. W. Watson, *J. Phys. Chem. C*, 2010, **114**, 2321–2328.

17 S. Y. Chen and L. W. Wang, *Appl. Phys. Lett.*, 2011, **99**, 222103.

18 E. Nurlaela, S. Ould-Chikh, M. Harb, S. D. Gobbo, M. Aouine, E. Puzenat, P. Sautet, K. Domen, J.-M. Basset and K. Takanabe, *Chem. Mater.*, 2014, **26**, 4812–4825.

19 S. J. Henderson and A. L. Hector, *J. Solid State Chem.*, 2006, **179**, 3518–3524.

20 J. Wang, T. Fang, L. Zhang, J. Feng, Z. Li and Zou, Z, *J. Catal.*, 2014, **309**, 291–299.

RSC Advances Accepted Manuscript

21 S. S. K. Ma, T. Hisatomi, K. Maeda, Y. Moriya and K. Domen, *J. Am. Chem. Soc.*, 2012, **134**, 19993–19996.

22 Y. Kado, R. Hahn and C.-Y. Lee, *Electrochem. Commun.*, 2012, **17**, 67–70.

23 Y. Kado, C. Y. Lee, K. Lee, J. Muller, M. Moll, E. Spiecker and P. Schmuki, *Chem. Commun.*, 2012, **48**, 8685–8687.

24 G. Kresse and J. Furthmüller, *Comput. Mater. Sci.*, 1996, **6**, 15–50.

25 J. P. Perdew, J. A. Chevary, S. H. Vosko, K. A. Jackson, M. R. Pederson, D. J. Singh and C. Fiolhais, *Phys. Rev. B*, 1992, **46**, 6671–6687.

26 H. J. Monkhorst and J. D. Pack, *Phys. Rev. B*, 1976, **13**, 5188−5192.

27 C. G. Van de Walle and J. Neugebauer, *J. Appl. Phys.*, 2004, **95**, 3851–3879.

28 X. Ma, Y. Dai, L. Yu and B. Huang, *Sci. Rep.*, 2014, **4**, 3986.

29 W. J. Yin, S. H. Wei, M. M. Al-Jassim, J. Turner and Y. F. Yan, *Phys. Rev. B*, 2011, **83**, 11.

30 S. Chen and L.-W. Wang, *Appl. Phys. Lett.*, 2011, **99**, 222103.

31 S. Lany and A. Zunger, *Phys. Rev. B*, 2008, **78**, 235104.

32 H. Shi and M.-H. Du, *Phys. Rev. B*, 2014, **90**, 174103.

33 P. Reunchan, S. Ouyang, N. Umezawa, H. Xu, Y. Zhang, and J. Ye, *J. Mater. Chem. A*, 2013, **1**, 4221–4227.

34 M. E. Grillo, S. D. Elliott and C. Freysoldt, *Phys. Rev. B*, 2011, **83**, 085208.

35 J. B. Varley, A. Janotti and C. G. Van de Walle, *Adv. Mater.*, 2011, **23**, 2343–2347.

36 B. A. Pinaud, A. Vailionis and T. F. Jaramillo, *Chem. Mater.*, 2014, **26**, 1576–1582.

37 A. Dabirian and R. van de Krol, *Appl. Phys. Lett.*, 2013, **102**, 033905.

38 J. L. Lyons, A. Janotti and C. G. Van de Walle, *Phys. Rev. Lett.*, 2012, **108**, 156403.



RSC Advances Accepted Manuscript

39 C. Freysoldt, B. Grabowski, T. Hickel, J. Neugebauer, G. Kresse, A. Janotti and C. G. Van de Walle, *Rev. Mod. Phys.*, 2014, **86**, 253–305.

40 W. J. Jo, J. W. Jang, K. J. Kong, H. J. Kang, J. Y. Kim, H. Jun, K. P. Parmar and J. S. Lee, *Angew. Chem., Int. Ed.*, 2012, **51**, 3147–3151.

41 D. K. Zhong, S. Choi and D. R. Gamelin, *J. Am. Chem. Soc.*, 2011, **133**, 18370–18377.

42 Y. B. Li, L. Zhang, A. Torres-Pardo, J. M. Gonzalez-Calbet, Y. H. Ma, P. Oleynikov, O. Terasaki, S. Asahina, M. Shima, D. Cha, L. Zhao, K. Takanabe, J. Kubota and K. Domen, *Nat. Commun.*, 2013, **4**, 2566.

43 J. Osorio-Guillén, S. Lany and A. Zunger, *Phys. Rev. Lett.*, 2008, **100**, 036601.

44 J. Feng, D. Cao, Z. Wang, W. Luo, J. Wang, Z. Li and Z. Zou, *Chemistry - A European Journal*, 2014, **20**, 16384–16390.

**Figure Captions**

**Figure 1** Accessible range of chemical potentials (blue line) under equilibrium growth conditions for $Ta_3N_5$. A (N-rich condition) and B (N-poor condition) sites are chosen as the representative chemical potentials for the following calculation of defect formation energy.

**Figure 2** Calculated formation energies of defects in $Ta_3N_5$ as a function of the Fermi energy under N-rich condition (a), and N-poor condition (b).

**Figure 3** Calculated total and projected density of states for $O_{N4}$ (a), $O_{N3}$ (b), $V_{N4}$ (c) and $V_{N3}$ (d). The red dashed lines indicate the Fermi level, which is set to zero.

**Figure 4** Calculated band decomposed charge-density for $V_{4N}$ (a) and $V_{3N}$ (b) with a 0.003 $eÅ^{-3}$ isosurface value.

**Figure 5** Calculated local density of states of N-N atom pair in interstitial N doped $Ta_3N_5$ (a)



RSC Advances Accepted Manuscript

and O-N atom pair in interstitial O doped $Ta_3N_5$ (b).

**Figure 6** Local geometric structures of interstitial N (a) and interstitial O (b) doped $Ta_3N_5$.

**Figure 7** The schematic level diagram of N-N atom pair in interstitial N doped $Ta_3N_5$ (b) and O-N atom pair in interstitial O doped $Ta_3N_5$ (b).

**Figure 8** Configuration coordinate diagram for $V_{4N}$ defect (a), $E_{opt}$ refers to the energy of optical transition. The formation energy as a function of Fermi level for $V_{4N}$ defect that can occur in two charge states: +1 and +2 (b).

RSC Advances Accepted Manuscript

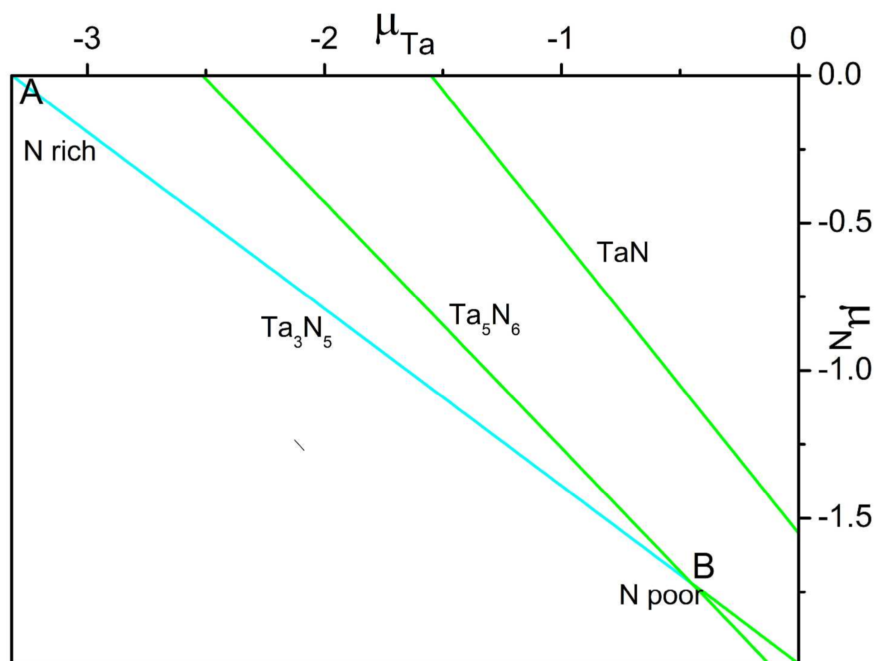


**Figure 1**

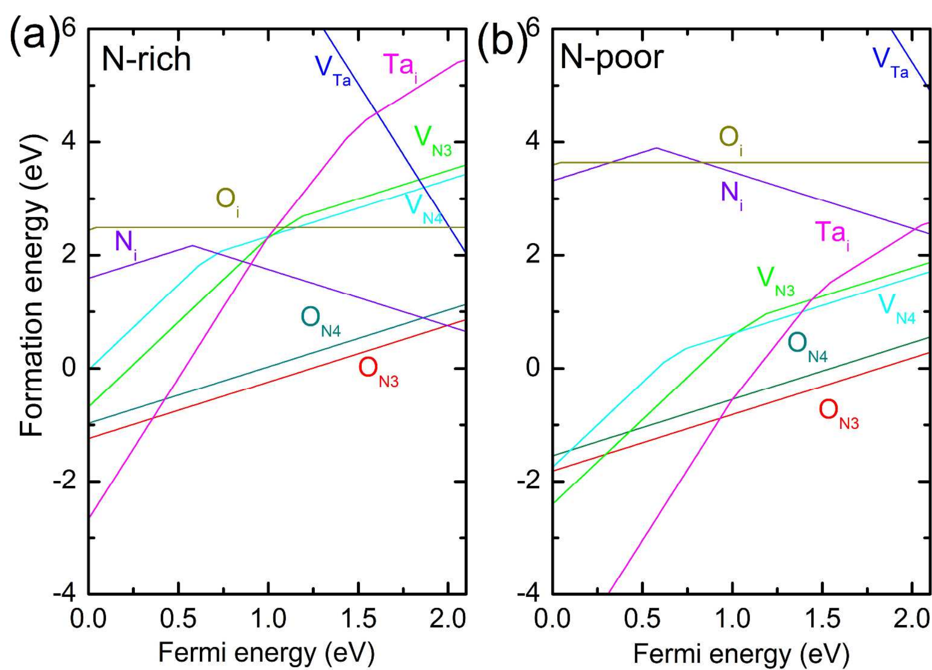


**Figure 2**

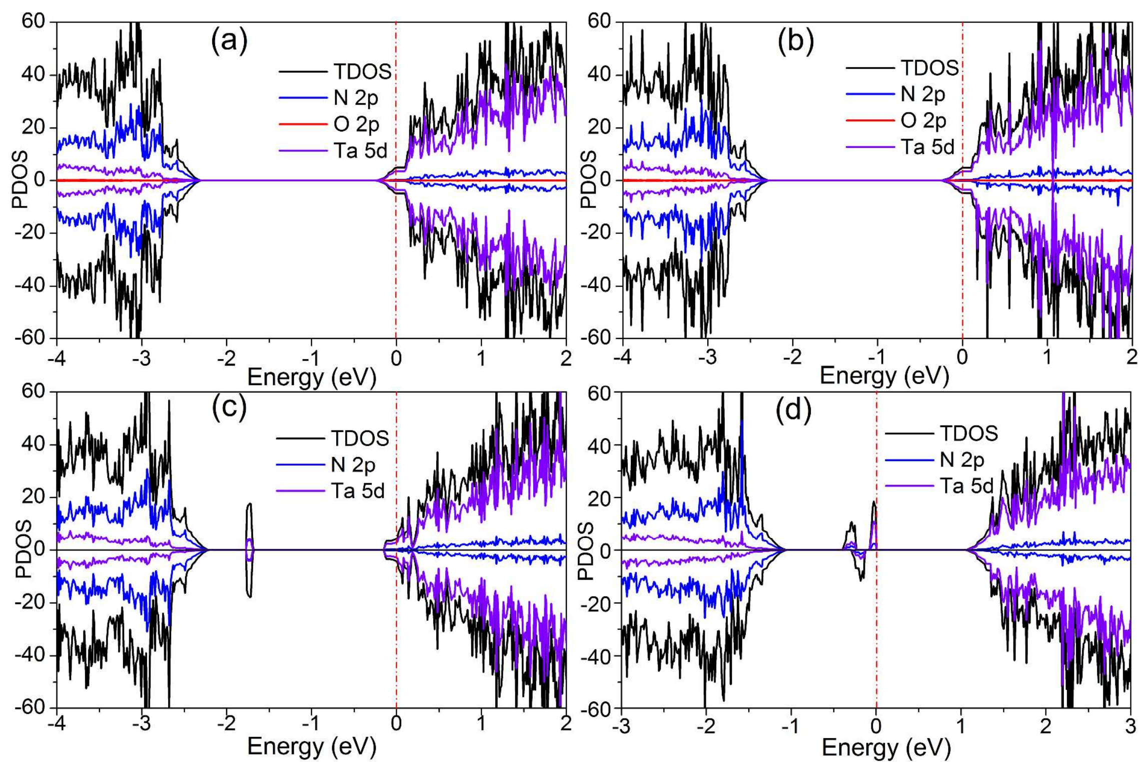


**Figure 3**



RSC Advances Accepted Manuscript

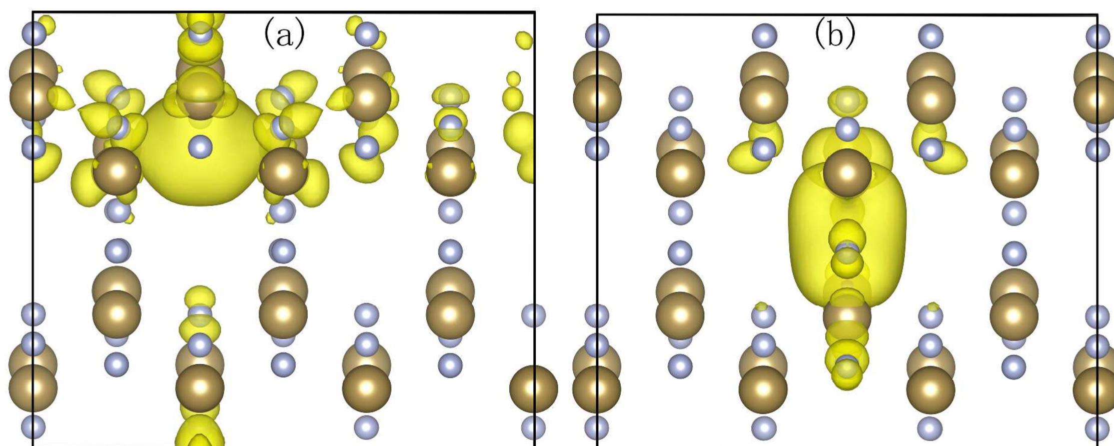


**Figure 4**

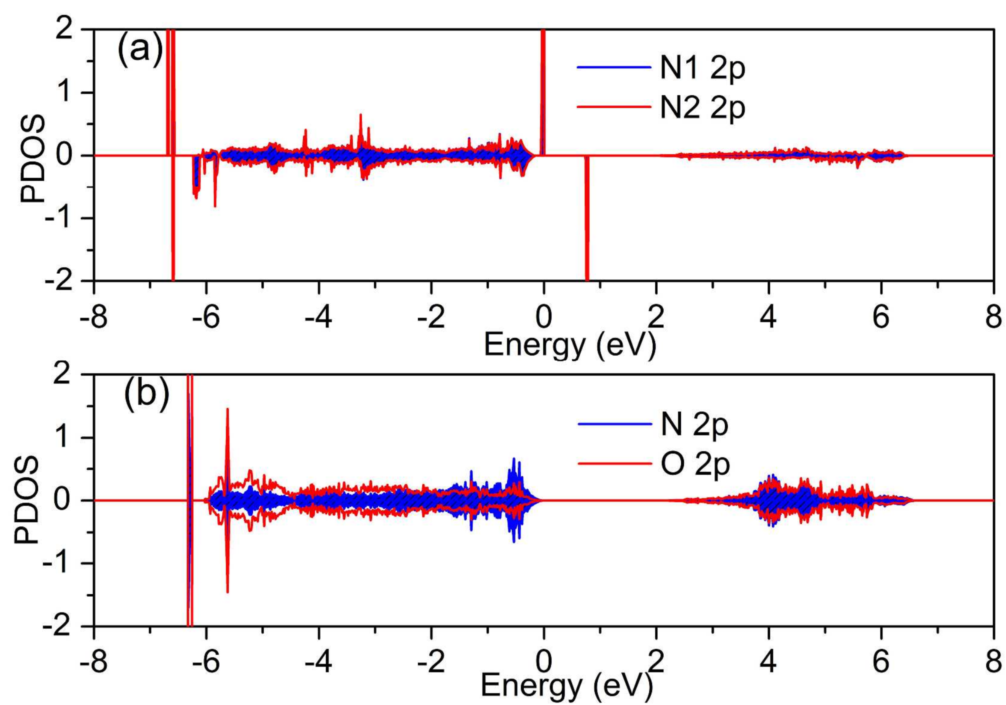


**Figure 5**

RSC Advances Accepted Manuscript

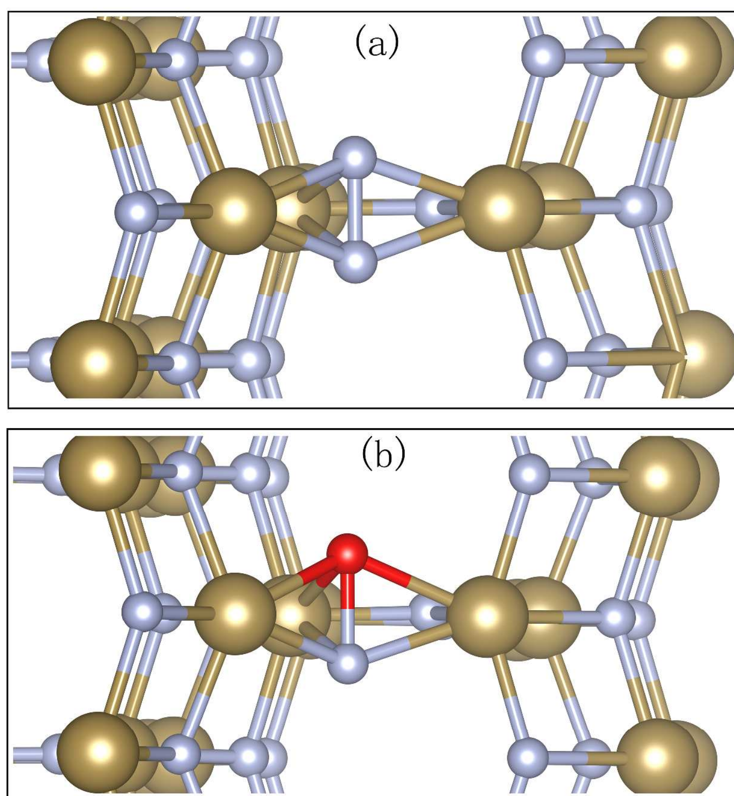


Figure 6

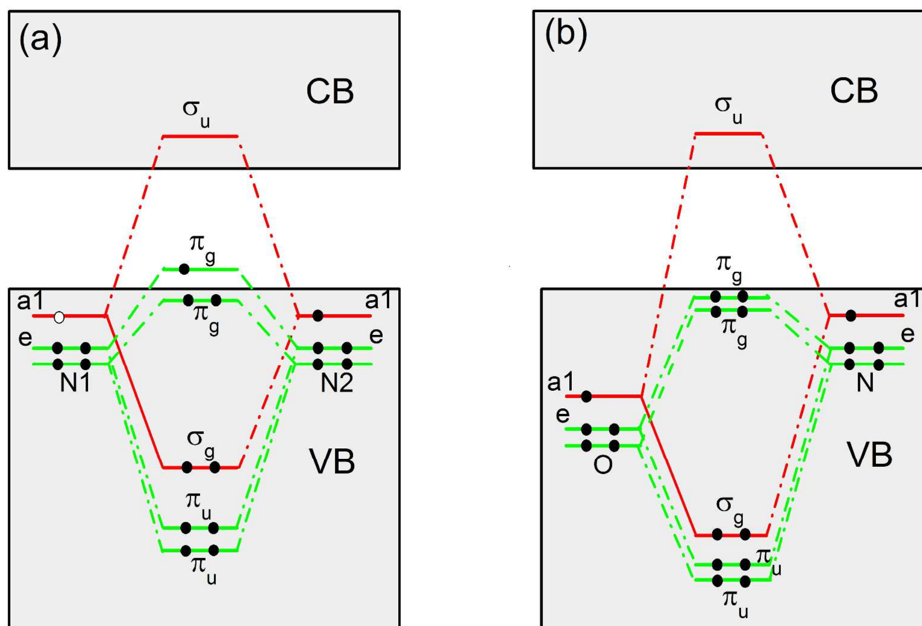


Figure 7



RSC Advances Accepted Manuscript

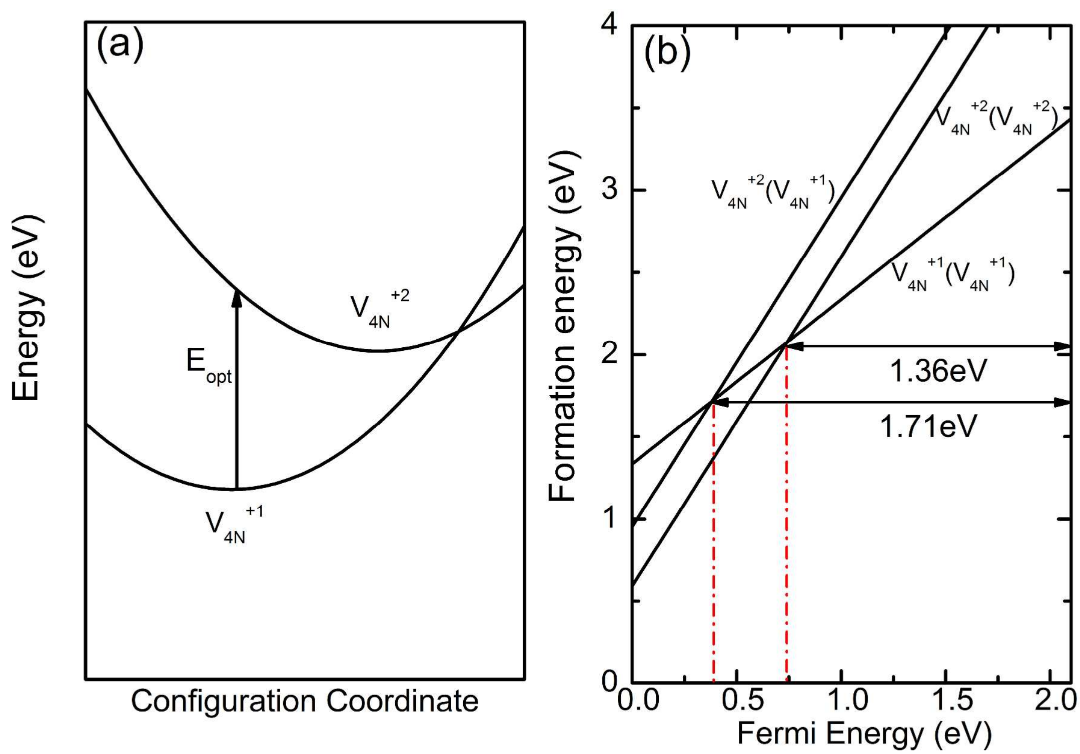


**Figure 8**



RSC Advances Accepted Manuscript